HEFAT2007
5th International Conference on Heat Transfer, Fluid Mechanics and Thermodynamics
Sun City, South Africa
Paper number: CC1

PREDICTING ACOUSTIC WAVE- FLOW IN A THERMOACOUSTIC RESONATOR WITH BINARY GAS- MIXTURES

C. F. Cheng [1] and Mohd. Ghazali N.[2]
[1]School of Engineering and Science, Curtin University of Technology Sarawak Campus,
CDT 250, 98009 Miri, Sarawak, Malaysia. chengcf@curtin.edu.my
[2]Faculty of Mechanical Engineering, Universiti Teknologi Malaysia (UTM Skudai).
81310 UTM Skudai, Johor, Malaysia. normah@utm.edu.my

ABSTRACT

This paper studies the trend of near- wall acoustic wave flow in a thermoacoustic resonator with noble gas mixtures. Dimensionless 2D N-S equations were solved numerically for acoustic waves in a rectangular chamber generated by a membrane acoustic driver. The dynamic viscosity and thermal thermal thermal conductivity for the fluid mixture were calculated using the *Wilke* and *Wassiljewa's* method while the gas mixture density is calculated using the virial equation of state. These parameters are incorporated into the *Re* and *Pr* number of the Navier-Stokes equations. Unsteady flow within the chamber is observed for different mixture combinations of He-Ar and He-Xe. The best mixture found is He-Xe (6:4) where thicker thermal boundary layer profile is observed near the solid surface. As time increases, vortex formation is found near the wavemaker, a similar phenomenon observed for pure fluid. This result shows potential for numerically predicting thermoacoustic behavior that involves mixtures.

INTRODUCTION

Thermoacoustic cooling Thermoacoustics is a phenomenon of temperature gradient generation when sound wave is impinged at a solid surface. N. Rott introduced modern of thermoacoustics theory which was further explained by G.W. Swift [1]. This linear theory of thermoacoustics has served as a fundamental framework for more research to be done and hence constantly providing improvement to such technologies. Although still in its infancy stage, the existing theory has enabled a few thermoacoustic coolers to be built. These include the Thermoacoustic Life Science Refrigerator (TALSR), Hofler's refrigerator, Wetzel and Herman's refrigerator and the latest, Swift's natural gas liquefier.

Due to the attractiveness of the technology, the research of thermoacoustics has gained more popularity. Thermocaoustic refrigerator which is a CFC free device promises a great alternative to conventional cooling. Many analytical, experimental and simulations have been carried out worldwide by various researchers to improve the technology.

In the development analytical study, Mozurkewich [2] claimed that Swift's assumption on having the same time-average temperature of the adjacent pore is true within the stack but not at the edge of the stack. It has been proved that the heat transfer is most intense at both side of the edge. Following that Mozurkewich has come out with a new one dimensional transverse heat transfer model in the thermoacoustics. This finding was found after a decade of Swift's published linear thermoacoustic theory which suggests that there are still many aspects of thermoacoustics that need to be understood. Meanwhile the contribution of computational work was pioneered by Knio and Worlikar [3] in 1996. In his earliest work, a low Mach number velocity stream function for flows within two parallel stack plates was modeled and simulated. While most of the computational work was focused within the stack regime, Mohd. Ghazali N. [4] performed numerical study for a full thermoacoustic resonator. The acoustic wave generation and propagation was observed. Blanc- Benon et al [5] performed both experimental and computational visualization of the flow field around stack plates.

With the need to find replacement for a sustainable environmental friendly cooling alternative, research into thermoaouctics is worthwhile. There are many aspects of thermoacoustics needed more understanding such as nonlinear acoustic effect, vortex, turbulence and acoustic streaming which is beyond the prediction of linear acoustic theory. Expensive experimental setup could lead numerical study to play a more prominent role in gaining better insights of flow characteristic and heat transfer behavior of acoustic wave around the stack region and also the resonator chamber itself.

Advantages Thermoacoustic technology is gaining popularity owing to its simplicity of mechanism. Simplest thermoacoustic device only requires a single electrically driven wave maker, used to generate oscillating acoustic signals and drives the thermal system of the device. The thermoacoustic core consists of stack plates, hot and cold heat exchanger (see Figure 1(a)). Sliding seals or lubrication are not needed for the system, which eases maintenance. Different from conventional refrigeration system, thermoacoustic device uses environmentally friendly working fluid, i.e. noble gases.

NOMENCLATURE

STP	[-]	Standard temperature and pressure
Re	[-]	Reynolds Number
Pr	[-]	Prandtl Number
ρ	[Kg/m^3]	Density of fluid
M	[-]	Mach number
Q	[-]	Nonlinear terms
T	[K]	Temperature
p	[N/m^2]	Pressure
R	[kJ/k.Mol-K]	Gas constant
C_p	[kJ/kg.K]	Specific heat capacity
μ	[kg/m.s]	Dynamic viscosity
k	[W/m.K]	Thermal thermal thermal conductivity
He	[-]	Helium
Ar	[-]	Argon
Xe	[-]	Xenon
c	[m/s]	Speed of sound
H	[m]	Width
L	[m]	Length
L/H	[-]	Aspect ratio of resonator
x	[-]	Dimensionless Cartesian axis direction
y	[-]	Dimensionless Cartesian axis direction
u	[-]	Dimensionless x- velocity
v	[-]	Dimensionless y- velocity
Special characters		
λ	[m]	Wavelength
δ	[m]	Viscous boundary layer
γ	[-]	Specific heat ratio of fluid
ω	[1/s]	Forcing frequency
ψ	[-]	Species type of noble gas
α	[-]	Mixture constant
β	[-]	Mixture constant
φ	[-]	Mixture constant
Subscripts		
1		Type 1
2		Type 2
v		Viscous
k		Thermal
mix		Mixture of binary
o		Ambient or reference
m		Mean value

How it works The working principle of standing wave thermoacoustic cooling is to provide heat-pumping effect. As opposed to the typical Carnot Cycle, this principle satisfies the Second Thermodynamic Laws on irreversibility and hence is proven feasible in continuously providing heat-pumping work to the system. The standing wave thermoacoustic heat pumping consists of four- step cycle, two adiabatic (step 1 and 3) and two constant- pressure heat transfer steps (step 2 and 4) each.

Initially, the acoustic wave drives the gas parcel forward, along the stack plates to a region with higher pressure which causes an increase of temperature in the gas particle due to the adiabatic compression. The temperature of the gas particle is now higher compared to the temperature of stack plate when it reached the other end of the stack plate. This caused heat transfer from the gas parcel to the plate to happen in an irreversible manner. After the transfer of heat energy, the temperature of gas parcel reduces. At the same time, it moves back to its initial position, where the region is of a lower pressure, causing its temperature to fall continuously below that of the stack. At the same time, the gas particle is said to experiences adiabatic expansion. Finally the gas parcels reached its initial position and once again, due to temperature gradient, heat transfer from stack plate to gas parcel occurs irreversibly. The cycle is then repeated by each of the gas parcels in the resonator chamber.

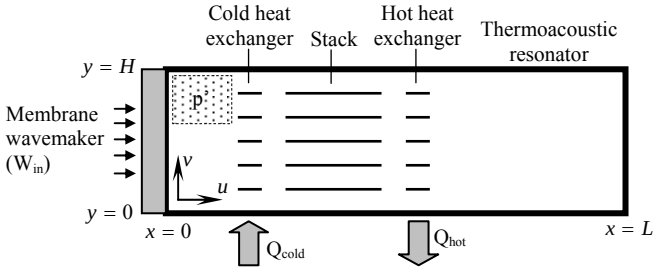

Figure 1 Components in a thermoacoustic refrigerator (p' denotes plot region);

Thermoacoustic effect In the thermoacoustic core, rapid movement of gas particles along the stack causes a temperature gradient along the stack plates, which generates the thermoacoustic effect. This effect takes place in the thin thermal boundary layer around the stack plate. The thermal penetration depth is the distance that the heat is able to diffuse through the working fluid in an oscillating cycle. In contrast to the thermal penetration depth, the viscous boundary layer reduces the kinetic energy of the working fluid. Equations (1) and (2) represent the viscous as well as the thermal penetration depth across a solid boundary [6].

$$\delta_v = \sqrt{\frac{2\mu}{\omega\rho}} \tag{1}$$

$$\delta_k = \sqrt{\frac{2k}{\omega\rho C_p}} \tag{2}$$

A working fluid with higher thermal thermal conductivity leads to the generation of larger thermal penetration layer, δ_k around the stack. This is why noble gases have been chosen as a favorable working fluid in thermoacoustic systems. Research from experimental and theoretical work even shows that binary mixture inert gas promises a better thermoacoustic cooling effect [6,7]. Studies have been carried out on mixtures of two or three noble gases in order to obtain a better thermoacoustic effects. Thermoacoustic Life Science Refrigerator (TALSR), owned by NASA was built by Garett (S.L. Garett in M. Wetzel and C. Herman, 1997) [6] with a mixture of 89% He and 11% Xe has achieved COP of 0.5, which is a factor of two as compared to a purely He system. Tijani et al [7] then did a further experimental study on the performance of every type of binary noble gas mixtures with He at different *Pr* numbers. The experimental result showed that highest COP achieved was 1.9 with 30% mixture of Xe in He. This numerical study will look into the effects of acoustic travelling wave flow and thermal behaviour of pure He and its binary mixtures between He-Ar and He- Xe at the ratio of 6:4.

NUMERICAL FORMULATION

Simulations of the unsteady flow are performed using a computational model that is an extended version of the scheme originally introduced Mohd. Ghazali N. [4]. A half-wave length rectangular chamber with a length of *L* and width of *H* is considered. The governing equations used to describe the motion of He and its mixture within the thermoacoustic chamber is the 2D unsteady N-S equations and state equations. A brief explanation of the scheme is described here while the details of the formulation should be referred to the mentioned reference.

To make them dimensionless, the variables are re-defined by dividing them by a constant reference property appropriate to the flow. The non-dimensional parameters are defined as following [4].

$$\bar{t} = t\omega, \qquad \bar{x} = \frac{x}{H}, \qquad \bar{y} = \frac{y}{H}, \qquad \bar{u} = \frac{u}{\omega H},$$

$$\bar{v} = \frac{v}{\omega H}, \quad \bar{\rho}_o = \frac{\rho_0}{\rho_m}, \qquad \bar{T} = \frac{T}{T_m}, \qquad \bar{p} = \frac{p}{\rho_m R T_m}$$

ω is the forcing frequency generated by the speaker, H is the width of the resonator, while ρ_m is the mean density and T_m represents the mean temperature in the domain. Next, a set of equations describing the mean flow are derived by decomposing flow variables ρ, p and T into their mean and fluctuation parts which are later introduced into the dimensionless N-S equations. The continuity equation is later separated into linear and nonlinear terms. The viscous dissipation terms in the energy equation is neglected on the basis of being less important for flow at high *Re* number. With Boussinesq assumption, the density in the nonlinear terms are neglected as its variation is small relative to its mean density. The continuity equation is finally used to eliminate the pressure term in the momentum and energy equations which results in the following set of equations. For convenience, all the overbar symbols are not shown.

$$\frac{\partial^2 u}{\partial t^2} = \frac{1}{M^2\gamma}\left(\frac{\partial^2 u}{\partial x^2} + \frac{\partial^2 v}{\partial x \partial y} - \frac{\partial^2 T}{\partial x \partial t}\right) + \frac{1}{Re}\frac{\partial}{\partial t}\left(\frac{\partial^2 u}{\partial x^2} + \frac{\partial^2 u}{\partial y^2}\right) + \frac{1}{3Re}\frac{\partial}{\partial t}\left(\frac{\partial^2 u}{\partial x^2} + \frac{\partial^2 v}{\partial x \partial y}\right) + \frac{1}{M^2\gamma}\frac{\partial}{\partial x}(Q_p) - \frac{\partial}{\partial t}(Q_x) \tag{3}$$

$$\frac{\partial^2 v}{\partial t^2} = \frac{1}{M^2\gamma}\left(\frac{\partial^2 u}{\partial x \partial y} + \frac{\partial^2 v}{\partial y^2} - \frac{\partial^2 T}{\partial y \partial t}\right) + \frac{1}{Re}\frac{\partial}{\partial t}\left(\frac{\partial^2 u}{\partial x^2} + \frac{\partial^2 u}{\partial y^2}\right) + \frac{1}{3Re}\frac{\partial}{\partial t}\left(\frac{\partial^2 u}{\partial x \partial y} + \frac{\partial^2 v}{\partial y^2}\right) + \frac{1}{M^2\gamma}\frac{\partial}{\partial y}(Q_p) - \frac{\partial}{\partial t}(Q_y) \tag{4}$$

$$\frac{\partial T}{\partial t} = \frac{\gamma}{RePr}\left(\frac{\partial^2 T}{\partial x^2} + \frac{\partial^2 T}{\partial y^2}\right) + (1-\gamma)\left(\frac{\partial u}{\partial x} + \frac{\partial v}{\partial y}\right) + (1-\gamma)Q_p - \gamma Q_T \tag{5}$$

$$\frac{\partial p}{\partial t} = \frac{\gamma}{\gamma - 1}\left[\frac{\partial T}{\partial t} - \frac{1}{RePr}\left(\frac{\partial^2 T}{\partial x^2} + \frac{\partial^2 T}{\partial y^2}\right) + Q_T\right] \tag{6}$$

where subscripted terms, *Q* contains the nonlinear components of each equations defined as following

$$Q_x = \rho\left(\frac{\partial u}{\partial t} + u\frac{\partial u}{\partial x} + v\frac{\partial u}{\partial y}\right) + u\frac{\partial u}{\partial x} + v\frac{\partial u}{\partial y} \tag{7}$$

$$Q_y = \rho\left(\frac{\partial v}{\partial t} + u\frac{\partial v}{\partial x} + v\frac{\partial v}{\partial y}\right) + u\frac{\partial v}{\partial x} + v\frac{\partial v}{\partial y} \tag{8}$$

$$Q_T = \rho\left(\frac{\partial T}{\partial t} + u\frac{\partial T}{\partial x} + v\frac{\partial T}{\partial y}\right) + u\frac{\partial T}{\partial x} + v\frac{\partial T}{\partial y} - \left(\frac{\gamma - 1}{\gamma}\right)\left(u\frac{\partial p}{\partial x} + v\frac{\partial p}{\partial y}\right) \tag{9}$$

$$Q_p = T\left(\frac{\partial p}{\partial t} + u\frac{\partial p}{\partial x} + v\frac{\partial p}{\partial y}\right) - p\left(\frac{\partial T}{\partial t} + u\frac{\partial T}{\partial x} + v\frac{\partial T}{\partial y}\right) + \left(u\frac{\partial p}{\partial x} + v\frac{\partial p}{\partial y}\right) + (p + T + pT)\left(\frac{\partial u}{\partial x} + \frac{\partial v}{\partial y}\right) \tag{10}$$

The dimensionless group of equations are the Mach number, Reynolds number and Prandtl number given as

$$M = \frac{\omega H}{\sqrt{\gamma R T_m}}, \qquad Re = \frac{\rho H^2 \omega}{\mu}, \qquad Pr = \frac{\mu C_p}{k}$$

The Finite Difference scheme is used in solving Equations (3) through (6) simultaneously to obtain *u, v, T* and *p*. The second order central spatial derivative is used to solve the interior grid point while one-sided derivatives are used to solve the boundary grids. Linear terms are solved using second order Crank- Nicholson method while the nonlinear terms are treated using Adam Bashford method. The second order linear temporal terms are approximated by second order central difference scheme while nonlinear terms are approximated by first order backward difference.

MIXTURE PARAMETERS

Mixture Pr number(Pr_{mix}) In calculating the *Pr* number of binary mixture, approach by F.W. Giacobbe [8] is used. For a binary mixture of components, *Pr* number is defined as

$$Pr_{mix} = \frac{\mu_{mix} C_{p_{mix}}}{k_{mix}} \tag{11}$$

Giacobbe [8] suggested the method by Wilke and Wassiljewa (in Giacobbe [8]) of estimating the mixtures' viscosity and thermal thermal thermal conductivity. These methods treat both the viscosity and thermal thermal thermal conductivity of a binary system as

$$\mu_{mix} = \left[\psi_1\mu_1 / (\psi_1 + \psi_2\alpha_{12}) + \psi_2\mu_2 / (\psi_2 + \psi_1\alpha_{21})\right] \tag{12}$$

$$k_{mix} = \left[\psi_1 k_1 /(\psi_1 + \psi_2\beta_{12}) + \psi_2 k_2 /(\psi_2 + \psi_1\beta_{21})\right] \quad (13)$$

where

$\alpha_{12} = \left[1 + (\mu_1/\mu_2)^{1/2}(m_2/m_1)^{1/4}\right]^2 / \left[8(1 + m_1/m_2\right]^{1/2}$,

$\alpha_{21} = (\mu_2/\mu_1)(m_1/m_2)\alpha_{12}$, and

$\beta_{12} = \varphi\alpha_{12}$ and $\beta_{21} = \varphi\alpha_{21}$

φ is a near unity chosen as 1 while α_{12} and α_{21} are functions which relate the gas molecular weight to the viscosities of each gas component in the mixture, and β_{12} and β_{21} relates the gas molecular weight to its pure component of thermal thermal thermal conductivity. The *Pr* number for a binary gas mixture is then given by

$$\mathrm{Pr}_{mix} = \frac{\left[\psi_1\mu_1 /(\psi_1 + \psi_2\alpha_{12}) + \psi_2\mu_2 /(\psi_2 + \psi_1\alpha_{21})\right] C_{p_{mix}}}{\left[\psi_1 k_1 /(\psi_1 + \psi_2\beta_{12}) + \psi_2 k_2 /(\psi_2 + \psi_1\beta_{21})\right]} \quad (14)$$

where, the specific heat capacity for a mixture is

$$C_{p_{mix}} = (5/2)\left[R/(\psi_1 m_1 + \psi_2 m_2)\right]. \quad (15)$$

Mixture Re number (Re_{mxs}) The *Re* number for a binary gas mixture as follows

$$Re_{mix} = \frac{\rho_{mix} H^2 \omega}{\mu_{mix}}, \quad (16)$$

where the density, ρ_{mix} and viscosity, μ_{mix} are now considered in its mixture form. In determining the binary mixtures' density, the *virial* equation of state is used. Consideration has been taken for the first three terms of the equations. A modified algorithm from Assael et al [9] is utilized to simulate the density of a binary gas mixture based on *virial* equation of state at various percentages of mixtures between He and other noble gases. The detail of the mixture of density formulation should therefore refer to the mentioned literature.

Defining $\omega = 2\pi f$, $f = c/\lambda$, $\lambda = 2L$ and $c = \sqrt{\gamma RT}$ and substituting these terms into Equation (16) and further rearranging yields the *Re* number for a mixture

$$Re_{mix} = \frac{\pi H^2 \rho_{mix}\sqrt{\gamma RT}}{L\mu_{mix}} \quad (17)$$

The value of π, γ and *R is defined as* $\pi = 3.142$, $\gamma = 1.667$ and $R = 8.314$ *kJ/kmol-K*. A FORTRAN program has been written to simulate the value of Pr_{mix} and Re_{mix} at different mixture compositions.

BOUNDARY CONDITIONS

The simulation domain considered is similar to **Figure 1**, except that the thermoacoustic core (stack and heat exchangers) are neglected. The inner wall of the thermoacoustic refrigerator is assumed to be adiabatic, non- slip, and non- penetrating. Meanwhile the *u* and *v* component velocities at the upper, lower and right boundaries are specified as zero. The acoustic input is introduced as $u(0,y,t)=U_0\, h(y) \sin t$. The ratio *L/H* is the aspect ratio where *L* and *H* are length and height of the thermoacoustic chamber respectively. U_0 and *h(y)* are the forcing amplitude and shape function respectively. Due to the use of a membrane wave maker, the value of the shape function *h* will be *h(y) =sin (y)*. In the simulation, generation and propagation of acoustic wave is used instead of direct standing wave. The reason is to observe the effects of propagation of travelling wave in the resonator filled with mixture. The membrane wave maker will generate a sinusoidal amplitude increment where maximum amplitude occurs at the centerline of the thermoacoustic chamber while minimum amplitude at both lower and uppermost positions of the chamber. The current simulation only considers a resonator without the presence of thermoacoustic core.

RESULTS AND DISCUSSIONS

Three cases were simulated to check the effect of binary gas mixtures, namely He (Re_{mix} =126724, Pr_{mix} =0.667), He-Ar (Re_{mix} =110516, Pr_{mix} =0.379) and He-Xe (Re_{mix} =113804, Pr_{mix} =0.191). These cases were run at STP with various values of Pr_{mix} and Re_{mix}. For all the cases, component ratio of the mixtures of He-Ar and He-Xe were fixed at 6:4, where the Pr_{mix} is found lowest (see Figure 3). Uniform grid is used throughout the domain with number of grids 400x100 made proportional to the aspect ratio of the thermoacoustic resonator. The choice of resolution is due to the limited computing capability.

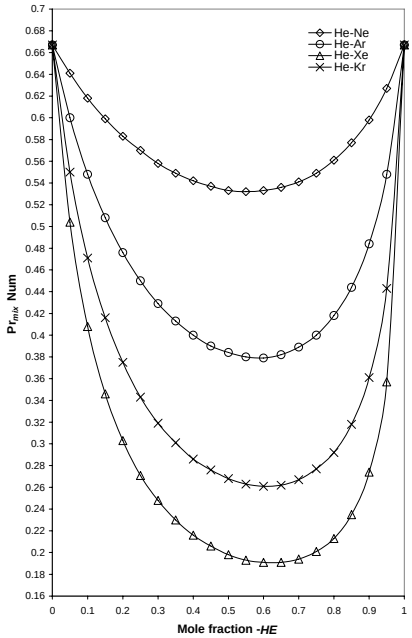

Figure 3 Pr_{mix} number at different percentage mixtures of He and other noble gases at *T*=300K.

Boundary Layer Profiles

In general, the axial velocity and temperature profiles throughout the resonator chamber seem to be similar for all the test cases considered. However, a closed-in view of the boundary layers of both the velocity and temperature profiles shows some differences. For velocity boundary layer profiles shown in **Figure 4**, variation on the profiles is not very obvious. All the three profiles seem to be almost intersecting each other.

Variations of the near wall thermal boundary layer profiles are obviously observed in **Figure 5**. As time progresses, the thermal boundary layer profiles for mixtures appear to be thicker profile than that of pure He. Among the trio, the thermal

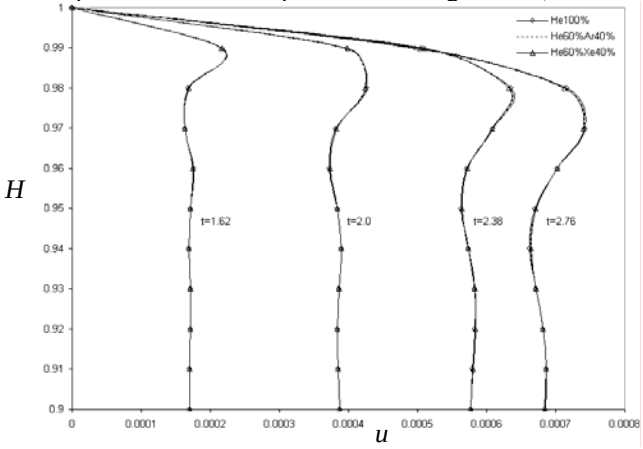

Figure 4 Axial velocity profiles for He, He-Ar *and* He-Xe*. (See plot area p' in Figure 1(a))*

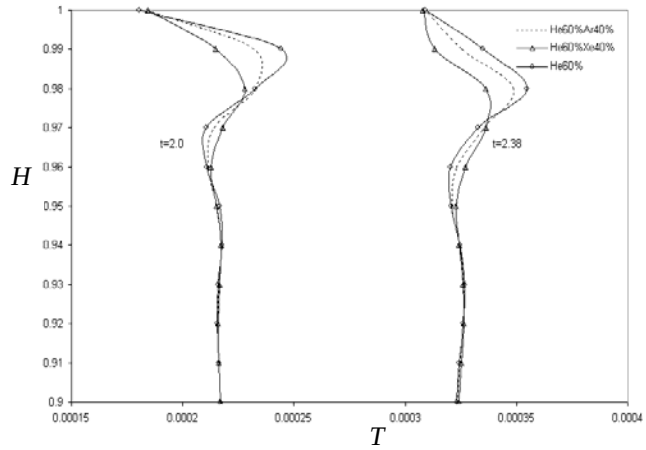

Figure 5 Temperature profiles for He, He-Ar and He-Xe*. (See plot area p' in Figure 1(a))*

boundary layer for He-Xe appears to be the thickest, followed by He-Ar. The result shows a positive indication of better performance of thermoacoustic refrigerator where thermal boundary layer is preferred to be larger than that of viscous boundary layer. Even if the viscous boundary layer does not change for either pure He or its binary mixture component, the thicker thermal boundary layer profile in binary mixture component itself is enough to suggest a better thermoacoustic effect. The increase of thermal boundary layer by reducing the *Pr* number has been discussed by *Schlichting* [10].

The results can be explained directly from two of the dimensionless parameter that influences the flow of acoustic wave, namely the Re_{mix} number and also Pr_{mix} number. The Re_{mix} for the pure component of inert gas and its binary mixture do not vary much considering the density of the mixture is almost the same. The only parameter, which causes difference in Re_{mix} is the viscosity of the mixture. Viscosity for pure He is lowest compared to its binary mixture with other inert gas.

Smaller viscosity causes higher inertia force in pure He compared to its binary mixtures. Thus, in **Figure 5**, the viscous boundary layer profile for pure component of He is more pronounced (thinner boundary layer profile) compared to its binary mixture He-Xe. The thermoacoustic effect is best explained by the dimensionless Pr_{mix} number itself, defined as

$$Pr_{mix} = \left(\frac{\delta_v}{\delta_k}\right)^2 = \frac{\mu_{mix} C_{pmix}}{k_{mix}} \qquad (18)$$

where the viscous penetration depth, δ_v of the fluid is the product of viscosity and isobaric specific heat capacity of the fluid, whilst the thermal penetration depth is directly proportional to the thermal conductivity of the fluid itself. Relating this relation to the cases of binary gas mixtures, the isobaric specific heat capacity for binary gas mixtures are lower compared to that of pure He (**Figure 6**) and this causes the reduction in Pr_{mix} number.

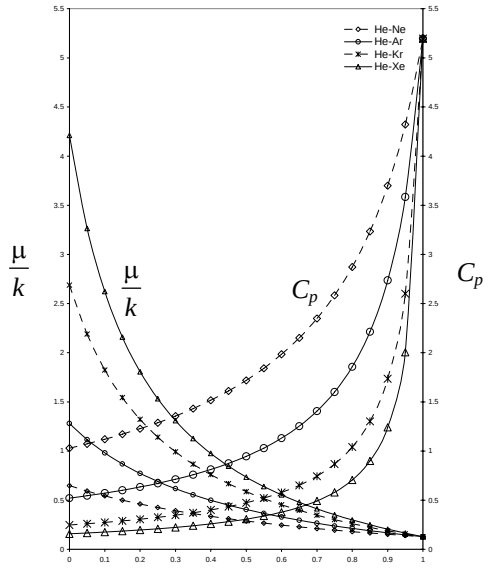

Figure 6 $\frac{\mu}{k}$ and C_p against mole fraction of He at 300K

For pure component Ne, Ar, Kr and Xe, their values of isobaric specific heat capacity are about 5 times less than that of pure component of He. Using mixture produced a greater reduction effect of δ_v than δ_k, so that the Pr number can be achieved as low as 0.191 for mixture of He-Xe at the ratio of 6: 4.

Pressure and Temperature Contours

Figures 7 and **8** show the contour plots of pressure and temperature in the entire resonator chamber. The area across the center of resonator of (red in colour imprint) implies a higher value in temperature and pressure. The plots suggest a good agreement of the perfect gas relation where area with higher pressure is proportional to the area with higher temperature.

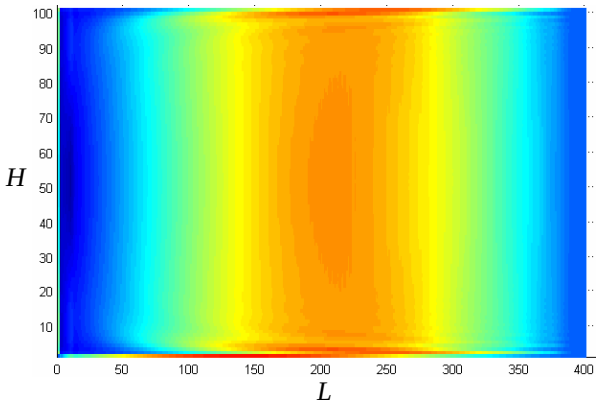

Figure 7 *Contour plot for pressure of* He-Xe *mixture at t=3.80.*

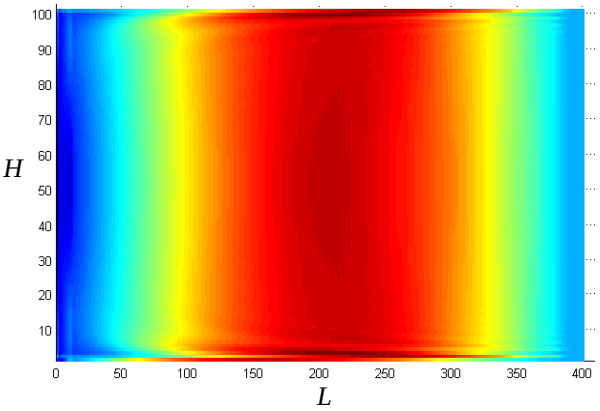

Figure 8 *Contour plot for temperature of* He-Xe *at t=3.80.*

Vortex Formation

As time progresses, the membrane acoustic driver is actually causing the formation of vortex near the left top and bottom corner of the resonator chamber. The formation of vortex on the top left corner of resonator chamber can be observed through the plots of velocity vector in **Figures 9**. Note that at t=3.42, the vortex seems to detach itself from the wall. At this time, the acoustic travelling wave is yet to reach the closed end of the resonator chamber. The oscillatory amplitude of membrane acoustic driver is maximized at the center of the resonator chamber while keeping an almost zero oscillation at the position of the top and bottom most of the chamber. This causes the velocity vectors to disperse to the upper and lower left area of the chamber where lower acoustic amplitude is generated. As time progresses flow rotation occurs and a vortex is formed. The effect of the vortex to the acoustic wave flow is not clearly understood.

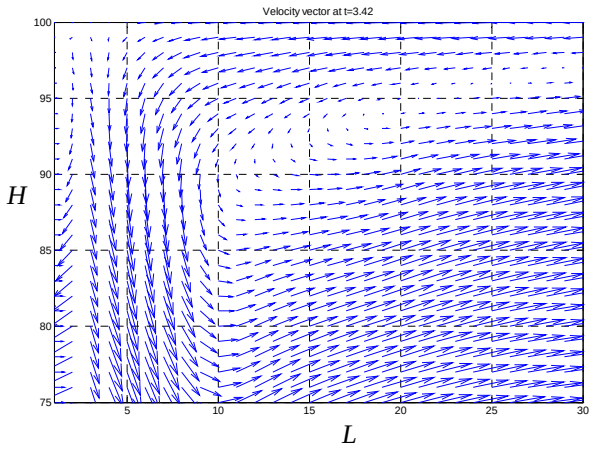

Figure 9 Vector plot for *He-Xe* at t=3.42.

CONCLUSION

Numerical study of 2D acoustic wave flow in a resonator chamber involving binary gas mixtures has been performed. The near wall thermal boundary layer profiles for mixture of He-Xe at ratio 6:4 has been found to be different than for pure He. Secondary flow of vortex formation was also observed near the membrane wave maker. Simulation shows the prediction and observation of the viscous and thermal boundary layer profiles are possible by using binary gas mixture's properties in the simulation. Future studies may include acoustic wave flows across the thermoacoustic core with mixtures.

REFERENCES

[1] G. W. Swift, Thermoacoustic Engines, J. Acoustic Soc. Am. 84(4), 1145-1180 (1988)

[2] G. Mozurkewich, A Model for Transverse Heat Transfer in Thermoacoustics, J. Acoustic Soc. Am 103(6), June 1998.

[3] A.-S. Worlikar, O.-M. Knio, Numerical Simulation of a Thermoacoustic refrigerator I. Unsteady Adiabatic Flow Around the Stack, J. Comput. Phys. Vol. 127, 424-451, 1996.

[4] Mohd. Ghazali, N., Numerical Simulation of Acoustic Wave in a Rectangular Chamber, PHD Dissertation, University of New Hampshire, USA. 2001.

[5] P. Blanc-Benon, E. Besnoin and O. Knio, Experimental and Computational Visualization of The Flow Field in A thermoacoustic Stack, C.R. Mecanique, 331 (17-24), 2003.

[6] M. Wetzel and C. Herman, Design Optimization of Thermoacoustic Refrigerators, International Journal of Refrigeration, Vol 20, No. 1:3-21, 1997.

[7] M.E.H. Tijani, J.C.H. Zeegers and A.T.A.M. de Waele, Prandtl Number and the Themoacoustic Refrigerators, J. Acoustic Soc. Am 112(1), July 2002.

[8] F.W. Giacobbe, Estimation of Prandtl Numbers in Binary Mixtures of Helium and other Noble Gases, J. Acoustic Soc. Am 96(6), Dec 1994.

[9] M.J. Assael, J.P. Matrin Trusler and Thomas F. Tsolakis, Thermophysical Properties of Fluids, Imperial College Press, 1996.

[10] H. Schlichting, Boundary Layer Theory, 7th Ed., McGraw Hill, USA, 1979.